Elastic waves in complex radially symmetric media

Youli Quan, Department of Geophysics, Stanford University*
Xiaofei Chen, Department of Earth Sciences, University of Southern California
Jerry M. Harris, Department of Geophysics, Stanford University

Summary

The generalized reflection and transmission coefficient method with modal expansion is developed to calculate the elastic wave field for the acoustic logging simulation and the crosswell seismic simulation in complex radially symmetric media. Our model consists of an arbitrary number of cylindrical layers and each cylindrical layer has arbitrary layers in the z-direction. This model can be used to simulate a variety of borehole geophysics problems: borehole casing with perforations, faults, source array, open and cased boreholes embedded in layered media, The simulation based on this method gives direct waves, reflections, transmissions, tube waves, tube wave conversions generated at casing perforations and horizontal interfaces, and the radiation pattern for a complicated borehole-formation structure.

Introduction

For most borehole simulations (e.g., Tubman et al., 1984; Chen et al., 1993), a borehole is simply modeled as cylindrical homogeneous layers. In a real borehole, however, the medium within a cylindrical layer usually are not homogeneous, whose elastic parameters usually change with depth. Pai et al. (1993) simulated the electromagnetic induction logging for this kind of models. The corresponding acoustic logging problems are more complicated, since we have to solve the elastodynamic equation in which both ***P*** and *S* waves are involved in. For elastic wave simulation, Bouchon (1993) and Dong et al. (1995) used the boundary element method for open and cased boreholes embedded in layered media, respectively. In this study, the generalized reflection and transmission coefficient method is developed to calculate more realistic models, such as multi-layered boreholes (casing and invaded zones) embedded in multi-layered formation, faults in the formation, and perforation in a casing. This semi-analytical approach is expected to be more flexible and efficient than pure numerical approaches.

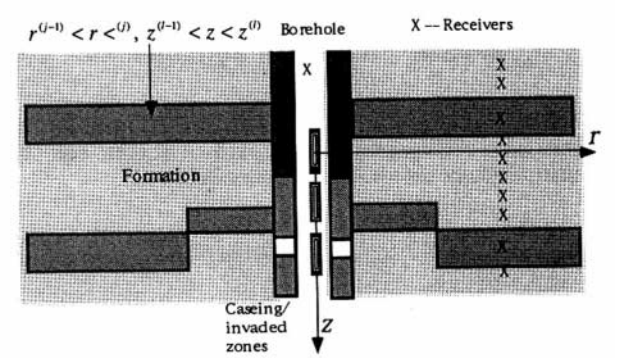

Figure 1. A complex radially symmetric model.

Governing equations

A general configuration of the problem considered in this study is shown in Figure 1, where the formation consists of several vertically heterogeneous cylinders, the source is located inside the borehole, while receivers are located either inside or outside the borehole. Although this model looks complicated, it still exhibits nice axial symmetric property. Taking the advantage of this symmetry we can derive a set of formulas to simulate the elastic wave propagation in this complex borehole-formation model. Since the model is radially symmetric, i.e., independent of θ in cylindrical coordinates, we can write the displacement for the jth cylindrical layer as

$$\mathbf{u}^{(j)} = \nabla\phi^{(j)} + \nabla\times(\mathbf{e}_\theta\psi^{(j)}), \tag{1}$$

where, $\phi^{(j)}$ and $\psi^{(j)}$ are ***P*** wave potential and *S* wave potential, respectively. To solve this problem, we expand these potentials by a set of eigenfunctions, $\{f_n^{(j)}(z), g_n^{(j)}(z); n=1,2,\ldots,N\}$, **as**

$$\begin{cases} \phi^{(j)}(r,z) = \sum_{n=1}^{N} \hat{\phi}_n^{(j)}(r) f_n^{(j)}(z) \\ \psi^{(j)}(r,z) = \sum_{n=1}^{N} \hat{\psi}_n^{(j)}(r) g_n^{(j)}(z) \end{cases}, \tag{2}$$

where the eigen-functions $f_n^{(j)}(z)$ and $g_n^{(j)}(z)$ satisfy

$$\frac{d^2 f_n^{(j)}(z)}{dz^2} + [k_\alpha^{(j)}(z)]^2 f_n^{(j)}(z) = [\gamma_n^{(j)}]^2 f_n^{(j)}(z), \tag{3a}$$

$$\frac{d^2 g_n^{(j)}(z)}{dz^2} + [k_\beta^{(j)}(z)]^2 g_n^{(j)}(z) = [\nu_n^{(j)}]^2 g_n^{(j)}(z). \tag{3b}$$

I

$\gamma_n^{(j)}$ and $\nu_n^{(j)}$ are the corresponding eigen-values to be determined. Equation (3) is an eigenvalue problem that will be solved in a later section. The general solutions for $\hat{\phi}_n^{(j)}$ and $\hat{\psi}_n^{(j)}$ are

$$\begin{cases} \hat{\phi}_n^{(j)} = c_{p+}^{(j)}(n) H_o^{(1)}(\gamma_n^{(j)} r) + c_{p-}^{(j)}(n) H_o^{(2)}(\gamma_n^{(j)} r), & (4a) \\ \hat{\psi}_n^{(j)} = c_{s+}^{(j)}(n) H_1^{(1)}(\nu_n^{(j)} r) + c_{s-}^{(j)}(n) H_1^{(2)}(\nu_n^{(j)} r), & (4b) \end{cases}$$

for $j > 1$, and

$$\begin{cases} \hat{\phi}_n^{(1)} = c^{(1)}(n) J_o(\gamma_n^{(1)} r) - \dfrac{iF(\omega)}{8\pi} f_n^{(1)*} H_o^{(1)}(\gamma_n^{(j)} r), & (4c) \\ \hat{\psi}_n^{(1)} = 0, & (4d) \end{cases}$$

for $j = 1$ (fluid layer). Here, sign "+" refers to the wave going outward, and "-" refers to the wave coming inward. Coefficients $c_{p\pm}^{(j)}$ **and** $c_{s\pm}^{(j)}$ are determined by imposing boundary conditions at $r = r^{(j)}, j = 1,2,\ldots,J$. Using these

Downloaded 01 Dec 2011 to 171.64.173.107. Redistribution subject to SEG license or copyright; see Terms of Use at http://segdl.org/

potential solutions, we finally obtain the displacements and stresses in solid cylindrical layers ($j > 1$) as,

$$U_p^{(j)}(r,z) = \sum_{n=1}^{2N+1}\sum_{l=1}^{2N+1}\sum_{q=1}^{4}\left\{E_{pq}^{(j)}(r;l,n)c_q^{(j)}(n)\right\}\exp(ik_l z), \quad (5)$$

where, $U_1^{(j)} = u_r^{(j)}$, $U_2^{(j)} = u_z^{(j)}$, $U_3^{(j)} = \sigma_r^{(j)}$ and $U_4^{(j)} = \sigma_z^{(j)}$; $c_{1,2}^{(j)} = c_{p-,+}^{(j)}$ and $c_{3,4}^{(j)} = c_{s-,+}^{(j)}$; and ($E_{pq}^{(j)}(r;l,n)$; p, q=1,2,3,4} are given in the' Appendix. In the fluid-filled borehole (j=1), the displacements and stresses are:

$$U_p^{(1)}(r,z) = \sum_{n=1}^{2N+1}\sum_{l=1}^{2N+1}\sum_{q=1}^{2}\left\{E_{pq}^{(1)}(r;l,n)\hat{c}_q^{(1)}(n)\right\}\exp(ik_l z), \quad (6)$$

where, $\hat{c}_1^{(1)} = c_1^{(1)} = c^{(1)}/2$ and $\hat{c}_2^{(1)} = c_2^{(1)} + s_+ = c^{(1)}/2 + s_+$; $s_+(n) = \frac{i}{8\pi}F(\omega)f_n^{(1)*}(z_s)$; and { $E_{pq}^{(1)}(r;l,n)$; p=1, 3 and q=1,2} are given in the Appendix.

Generalized reflection and transmission matrices and frequency domain solution

To effectively determine the unknown coefficients, c(j), we introduce the generalized reflection and transmission matrices, $\hat{\mathbf{R}}_{+-}^{(j)}$ and $\hat{\mathbf{T}}_{+}^{(j)}$, via the following factorizations:

$$\begin{cases}\mathbf{C}_+^{(j+1)} = \hat{\mathbf{T}}_+^{(j)}\mathbf{C}_+^{(j)} \\ \mathbf{C}_-^{(j)} = \hat{\mathbf{R}}_{+-}^{(j)}\mathbf{C}_+^{(j)}\end{cases}, \quad (7a)$$

for j> 1 (solid-solid interface), and

$$\begin{cases}\mathbf{C}_+^{(2)} = \hat{\mathbf{T}}_+^{(1)}(\mathbf{C}_+^{(1)} + s+) \\ \mathbf{C}_-^{(1)} = \hat{\mathbf{R}}_{+-}^{(1)}(\mathbf{C}_+^{(1)} + s+)\end{cases} \quad (7b)$$

for j=1 (liquid-solid interface). By imposing the boundary conditions at each interface, we obtain fhe following recursive formulas,

$$\begin{cases}\hat{\mathbf{R}}_{+-}^{(N+1)} = \mathbf{0} \\ \hat{\mathbf{T}}_+^{(j)} = [\mathbf{I} - \mathbf{R}_{-+}^{(j)}\hat{\mathbf{R}}_{+-}^{(j+1)}]^{-1}\mathbf{T}_+^{(j)}, \\ \hat{\mathbf{R}}_{+-}^{(j)} = \mathbf{R}_{+-}^{(j)} + \mathbf{T}_-^{(j)}\hat{\mathbf{R}}_{+-}^{(j+1)}\hat{\mathbf{T}}_+^{(j)}\end{cases} \quad (8)$$

forj = N, N-l, ... 2,1.

Here, I is the unit matrix; $\mathbf{T}_+^{(j)}$, $\mathbf{T}_-^{(j)}$, $\mathbf{R}_{-+}^{(j)}$ and $\mathbf{R}_{+-}^{(j)}$ are given by

$$\begin{bmatrix}\mathbf{R}_{+-}^{(j)} & \mathbf{T}_-^{(j)} \\ \mathbf{T}_+^{(j)} & \mathbf{R}_{-+}^{(j)}\end{bmatrix} = \begin{bmatrix}\mathbf{E}_{11}^{(j)} & \mathbf{E}_{12}^{(j)} & -\mathbf{E}_{13}^{(j+1)} & -\mathbf{E}_{14}^{(j+1)} \\ \mathbf{E}_{21}^{(j)} & \mathbf{E}_{22}^{(j)} & -\mathbf{E}_{23}^{(j+1)} & -\mathbf{E}_{24}^{(j+1)} \\ \mathbf{E}_{31}^{(j)} & \mathbf{E}_{32}^{(j)} & -\mathbf{E}_{33}^{(j+1)} & -\mathbf{E}_{34}^{(j+1)} \\ \mathbf{E}_{41}^{(j)} & \mathbf{E}_{42}^{(j)} & -\mathbf{E}_{43}^{(j+1)} & -\mathbf{E}_{44}^{(j+1)}\end{bmatrix}^{-1}$$

$$\begin{bmatrix}-\mathbf{E}_{13}^{(j)} & -\mathbf{E}_{14}^{(j)} & \mathbf{E}_{11}^{(j+1)} & \mathbf{E}_{12}^{(j+1)} \\ -\mathbf{E}_{23}^{(j)} & -\mathbf{E}_{24}^{(j)} & \mathbf{E}_{21}^{(j+1)} & \mathbf{E}_{22}^{(j+1)} \\ -\mathbf{E}_{33}^{(j)} & -\mathbf{E}_{34}^{(j)} & \mathbf{E}_{31}^{(j+1)} & \mathbf{E}_{32}^{(j+1)} \\ -\mathbf{E}_{43}^{(j)} & -\mathbf{E}_{44}^{(j)} & \mathbf{E}_{41}^{(j+1)} & \mathbf{E}_{42}^{(j+1)}\end{bmatrix}_{r=r^{(j)}} \quad (9a)$$

and

$$\begin{bmatrix}\mathbf{R}_{+-}^{(1)} & \mathbf{T}_-^{(1)} \\ \mathbf{T}_+^{(1)} & \mathbf{R}_{-+}^{(1)}\end{bmatrix} = \begin{bmatrix}\mathbf{E}_{11}^{(1)} & -\mathbf{E}_{13}^{(2)} & -\mathbf{E}_{14}^{(2)} \\ \mathbf{E}_{31}^{(1)} & -\mathbf{E}_{33}^{(2)} & -\mathbf{E}_{34}^{(2)} \\ \mathbf{0} & -\mathbf{E}_{43}^{(2)} & -\mathbf{E}_{44}^{(2)}\end{bmatrix}^{-1}\begin{bmatrix}-\mathbf{E}_{13}^{(1)} & \mathbf{E}_{11}^{(2)} & \mathbf{E}_{12}^{(2)} \\ -\mathbf{E}_{33}^{(1)} & \mathbf{E}_{31}^{(2)} & \mathbf{E}_{32}^{(2)} \\ \mathbf{0} & \mathbf{E}_{41}^{(2)} & \mathbf{E}_{42}^{(2)}\end{bmatrix}_{r=r^{(1)}} \quad (9b)$$

Using the generalized R/T matrices we can easily obtain the coefficient vectors $\mathbf{C}_\pm^{(j)}$ as

$$\mathbf{C}_+^{(1)} = \mathbf{C}_-^{(1)} = (\mathbf{I} - \mathbf{R}_{+-}^{(1)})^{-1}\mathbf{R}_{+-}^{(1)}\mathbf{s}_+, \quad (10a)$$

and

$$\begin{cases}\mathbf{C}_+^{(j)} = \hat{\mathbf{T}}_+^{(j-1)}\hat{\mathbf{T}}_+^{(j-2)}\ldots\hat{\mathbf{T}}_+^{(1)}(\mathbf{I} - \hat{\mathbf{R}}_{+-}^{(1)})^{-1}\mathbf{s}_+ \\ \mathbf{C}_-^{(j)} = \hat{\mathbf{R}}_{+-}^{(j)}\mathbf{C}_+^{(j)}\end{cases}, \quad (10b)$$

for j>1. Once having the coefficients $\mathbf{C}_\pm^{(j)}$ we can calculate the frequency domain solutions (displacements and stresses) using equations (5) and (6). The corresponding time domain solution can be obtained by performing inverse Fourier transform.

Determination of eigen-functions

Let us now solve equation (3). First, we expand $f_n^{(j)}$ and $g_n^{(j)}$ as

$$\begin{cases}f_n^{(j)}(z) = \sum_{l=1}^{2N+1} a_p(n,l)\exp(ik_l z) \\ g_n^{(j)}(z) = \sum_{l=1}^{2N+1} a_s(n,l)\exp(ik_l z)\end{cases}; \quad (11)$$

then substituting equation (11) into (3), we obtain

$$\sum_{l=1}^{2N+1}\left\{[k_{\alpha,\beta}^{(j)}(z)]^2 - (\gamma_n^{(j)})^2 - (k_l)^2\right\}a_{p,s}^{(j)}(l,n)e^{ik_l z} = 0. \quad (12)$$

To solve this eigen-value problem, we assume that the vertically heterogeneity of each cylinder can be approximately expressed by Fourier series as

$$[k_{\alpha,\beta}^{(j)}(z)]^2 \approx \frac{1}{2\pi}\sum_{m=1}^{2N+1} w_{\alpha,\beta}^{(j)}(m)\exp(ik_m z), \quad (13)$$

with

$$w_{\alpha,\beta}^{(j)}(m) \int_{-L/2}^{+L/2}[k_{\alpha,\beta}^{(j)}(z)]^2\exp(-ik_m z)dz, \quad (14)$$

Downloaded 01 Dec 2011 to 171.64.173.107. Redistribution subject to SEG license or copyright; see Terms of Use at http://segdl.org/

Here, $k_n = 2\pi(l-N-1)/L$, and $L = z_M - z_0$ is the periodic length whose value should be larger enough to keep the final time domain solution to be correct in the given time window (Chen et al., 1993). Now equation (12) can be reduced to

$$\begin{cases}[\mathbf{A}^{(j)} - (\gamma_n^{(j)})^2 \mathbf{I}]\mathbf{a}_p^{(j)}(n) = 0 \\ [\mathbf{B}^{(j)} - (\nu_n^{(j)})^2 \mathbf{I}]\mathbf{a}_s^{(j)}(n) = 0 \end{cases}. \quad (15)$$

where,

$$\mathbf{a}_{p,s}^{(j)}(n) = [a_{p,s}^{(j)}(1,n), a_{p,s}^{(j)}(2,n), \ldots, a_{p,s}^{(j)}(2N+1,n)]^T, \quad (16)$$

and

$$\begin{cases} A_{ml}^{(j)} = -(k_m)^2 \delta_{lm} + w_\alpha^{(j)}(m-l) \\ B_{ml}^{(j)} = -(k_m)^2 \delta_{lm} + w_\beta^{(j)}(m-l) \end{cases}. \quad (17)$$

Finally, eigen-values $(\gamma_n^{(j)})^2$ and $(\nu_n^{(j)})^2$, and the corresponded cigen-vectors $\mathbf{a}_p^{(j)}(n)$ and $\mathbf{a}_s^{(j)}(n)$ can be obtained by using standard linear algebra programs.

Examples

An extreme case is a trivial case in which all cylindrical layers are homogeneous. The more general algorithm in this study should provide an identical solution to the one which is directly solved for this special case (see Chen et al.. 1993). Let $k_{\alpha\alpha}^{(j)}(z) = k_\alpha^{(j)}$ and $k_\beta^{(j)}(z) = k_\beta^{(j)}$ be constants, then from equation (15) we obtain

$$\begin{cases} (\gamma_n^{(j)})^2 = (k_\alpha^{(j)})^2 - k_n^2 \\ a_p^{(j)}(l,n) = \delta_{ln} \end{cases}, \quad (18a)$$

and

$$\begin{cases} (\nu_n^{(j)})^2 = (k_\beta^{(j)})^2 - k_n^2 \\ a_s^{(j)}(l,n) = \delta_{ln} \end{cases}. \quad (18b)$$

Substituting these special solutions into equations (5) and (6), we can obtain identical formulas with the solutions in Chen et al. (1993).

We present two crosswell profiling examples to show the applicability of this method for modeling waves in various complex boreholes. In these examples the seismograms are U_r component. Figure 2 is a common receiver gather sorted from a complete crosswell data set. There are 50 sources and 50 receivers. The source interval and receiver interval are all 2 m. The moveout of the tube wave in a common receiver gather is very different from that in a common source gather. In this example we include a cased borehole and a layer with fault. This synthetic data set can be used to test tomography techniques and other inversion methods. Tests of this kind can help us to understand the borehole effects on the inversion. Figure 3 shows an example of cased borehole with a perforation. To simulate how a perforation in a casing creates tube conversions, we put a low velocity layer in the casing. Tube wave to *P* and *S* conversions clearly show up in Figure 3a.

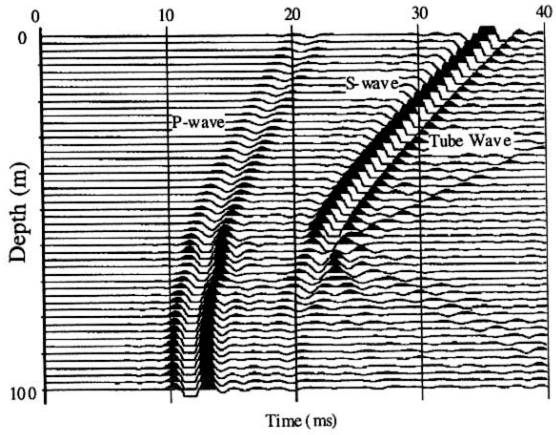

(a) Synthetic seismograms. The peak frequency of the source wavelet is 300 Hz.

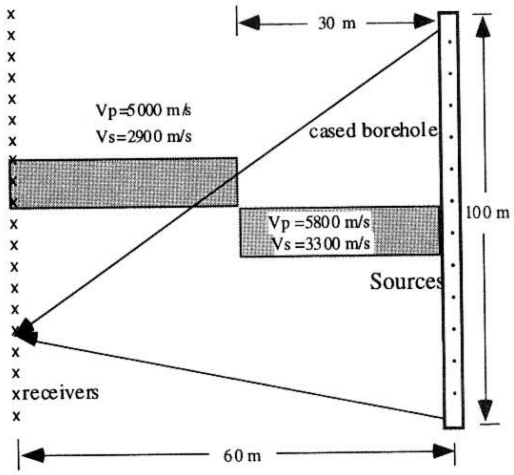

(b) Model geometry and parameters used for (a)

Figure 2. A common receiver gather sorted from a complete synthetic crosswell data set.

Conclusions

We have developed a semi-analytical approach to simulate the haves in a complex borehole-formation model in which there exist both cylindrical and horizontal layers. In this approach, we first calculation the eigen-functions of horizontal layers for each cylindrical layer. Then. we expand the wave equation solutions into these eigen-functions and apply the generalized reflection and transmission matrix method to solve the boundary problem for radial layers. Numerical examples show that this approach provides an effective tool to simulate complex models which are found in horehole modeling.

Downloaded 01 Dec 2011 to 171.64.173.107. Redistribution subject to SEG license or copyright; see Terms of Use at http://segdl.org/

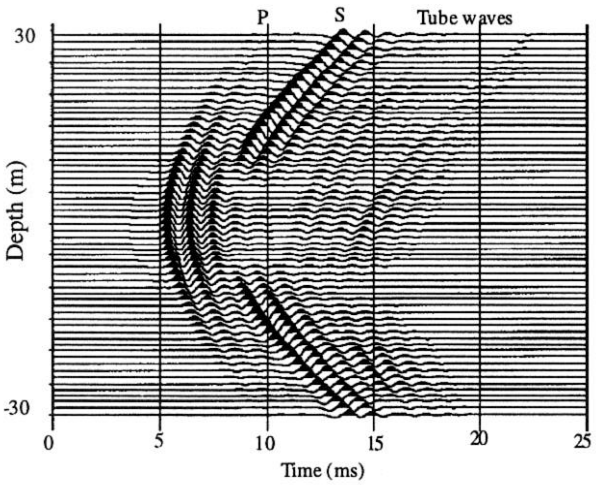

(a) Synthetic seismograms in common source gather. The peak frequency of the source wavelet is 1000 Hz.

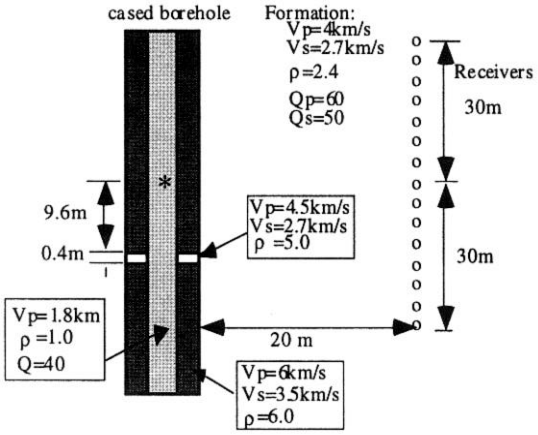

(b) Model geometry and parameters used for (a)

Figure 3. Test on the effect of casing perforation. It can be seen that the tube wave converts to *P* and *S* waves at a perforation.

References

Bouchon. M., 1993. A numerical simulation of the acoustic and elastic wavefields radiated by a source on a fluid-filled borehole embedded in layered medium: Geophysics, 58, No. 4, 475-481.

Chen, X, Quan, Y and Harris, M. J., 1994. Seismogram synthesis for radially layered media using the generalized reflection/transmission coefficients method: Expanded Abstracts of the 64th SEG annual meeting.

Dong, W., Bouchon. M. and Toksöz, M. N.. 1995, Borehole seismic-source radiation in layered isotropoc and anisotropic media: Boundary element modeling: Geophysics, 60. No. 3

Pai, D. M., Ahmad. J. and Kennedy W. D., 1993, Two-dimensional induction log modeling using a coupled-mode, multiple-reflection series method: Geophysics, 58, No. 4. 466.474.

Tubman, K. M., Cheng. C. H. and Toksöz, M. N., 1984. Synthetic full waveform acoustic logs in cased boreholes: Geophysics, 49, 1051-1059.

Appendix

For j>1 the elements $E_{p,q}^{(J)}$ in equation (5) are:

$$E_{11}^{(J)}(r;l,n) = -\gamma_n^{(J)} H_1^{(2)}(\gamma_n^{(J)} r) a_p^{(J)}(l,n),$$
$$E_{12}^{(J)}(r;l,n) = -ik_l H_1^{(1)}(\nu_n^{(J)} r) a_s^{(J)}(l,n),$$
$$E_{13}^{(J)}(r;l,n) = -\gamma_n^{(J)} H_1^{(1)}(\gamma_n^{(J)} r) a_p^{(J)}(l,n),$$
$$E_{14}^{(J)}(r;l,n) = -ik_l H_1^{(1)}(\nu_n^{(J)} r) a_s^{(J)}(l,n),$$
$$E_{21}^{(J)}(r;l,n) = ik_l H_o^{(2)}(\gamma_n^{(J)} r) a_p^{(J)}(l,n),$$
$$E_{22}^{(J)}(r;l,n) = \nu_n^{(J)} H_o^{(2)}(\nu_n^{(J)} r) a_s^{(J)}(l,n),$$
$$E_{23}^{(J)}(r;l,n) = ik_l H_o^{(1)}(\gamma_n^{(J)} r) a_p^{(J)}(l,n),$$
$$E_{22}^{(J)}(r;l,n) = \nu_n^{(J)} H_o^{(1)}(\nu_n^{(J)} r) a_s^{(J)}(l,n),$$
$$E_{31}^{(J)}(r;l,n) = \sum_{m=1}^{2N+1} \{[2k_m^2 H_o^{(2)}(\gamma_n^{(J)} r) + \frac{2\gamma_n^{(J)}}{r} H_1^{(2)}(\gamma_n^{(J)} r)]$$
$$\mu_{lm}^{(J)} a_p^{(J)}(m,,n) - \omega^2 H_o^{(2)}(\gamma_n^{(J)} r) \rho_{lm}^{(J)} a_p^{(J)}(m,n)\},$$
$$E_{32}^{(J)}(r;l,n) = \sum_{m=1}^{2N+1} [-i2k_m \nu_n^{(J)} \dot{H}_1^{(2)}(\nu_n^{(J)} r) \mu_{lm}^{(J)} a_s^{(J)}(m,n)],$$
$$E_{33}^{(J)}(r;l,n) = \sum_{m=1}^{2N+1} \{[2k_m^2 H_o^{(1)}(\gamma_n^{(J)} r) + \frac{2\gamma_n^{(J)}}{r} H_1^{(1)}(\gamma_n^{(J)} r)]$$
$$\mu_{lm}^{(J)} a_p^{(J)}(m,,n) - \omega^2 H_o^{(1)}(\gamma_n^{(J)} r) \rho_{lm}^{(J)} a_p^{(J)}(m,n)\},$$
$$E_{34}^{(J)}(r;l,n) = \sum_{m=1}^{2N+1} [-i2k_m \nu_n^{(J)} \dot{H}_1^{(1)}(\nu_n^{(J)} r) \mu_{lm}^{(J)} a_s^{(J)}(m,n)],$$
$$E_{41}^{(J)}(r;l,n) = \sum_{m=1}^{2N+1} [-i2k_m \gamma_n^{(J)} H_1^{(2)}(\gamma_n^{(J)} r) \mu_{lm}^{(J)} a_p^{(J)}(m,n)],$$
$$E_{42}^{(J)}(r;l,n) = \sum_{m=1}^{2N+1} [2k_m^2 \mu_{lm}^{(J)} - \omega^2 \rho_{lm}^{(J)}] H_1^{(2)}(\nu_n^{(J)} r) a_s^{(J)}(m,n)],$$
$$E_{43}^{(J)}(r;l,n) = \sum_{m=1}^{2N+1} [-i2k_m \gamma_n^{(J)} H_1^{(1)}(\gamma_n^{(J)} r) \mu_{lm}^{(J)} a_p^{(J)}(m,n)],$$
$$E_{44}^{(J)}(r;l,n) = \sum_{m=1}^{2N+1} [2k_m^2 \mu_{lm}^{(J)} - \omega^2 \rho_{lm}^{(J)}] H_1^{(1)}(\nu_n^{(J)} r) a_s^{(J)}(m,n)],$$

where $\mu_{lm}^{(J)} = \int_{-L/2}^{+L/2} \mu^{(J)}(z) \exp[i(k_l - k_m)z] dz$.

For j=1 the elements E_{pq} in equation (6) are:

$$E_{11}^{(1)}(r;l,n) = -\gamma_n^{(1)} H_1^{(2)}(\gamma_n^{(1)} r) a_p^{(1)}(l,n),$$
$$E_{12}^{(1)}(r;l,n) = -\gamma_n^{(1)} H_1^{(1)}(\gamma_n^{(1)} r) a_p^{(1)}(l,n),$$
$$E_{21}^{(1)}(r;l,n) = ik_l H_o^{(2)}(\gamma_n^{(1)} r) a_p^{(1)}(l,n),$$
$$E_{22}^{(J)}(r;l,n) = ik_l H_o^{(1)}(\gamma_n^{(J)} r) a_p^{(J)}(l,n),$$
$$E_{31}^{(1)}(r;l,n) = -\lambda^{(1)} (k_\alpha^{(1)})^2 H_o^{(2)}(\gamma_n^{(1)} r) a_p^{(1)}(l,n),$$
$$E_{32}^{(1)}(r;l,n) = -\lambda^{(1)} (k_\alpha^{(1)})^2 H_o^{(1)}(\gamma_n^{(1)} r) a_p^{(1)}(l,n).$$

Downloaded 01 Dec 2011 to 171.64.173.107. Redistribution subject to SEG license or copyright; see Terms of Use at http://segdl.org/